3852–3866 *Nucleic Acids Research, 2022, Vol. 50, No. 7* *Published online 25 March 2022*
https://doi.org/10.1093/nar/gkac196

H3K56 deacetylation and H2A.Z deposition are required for aberrant heterochromatin spreading

Chengcheng Zhang[1], Yuan Tian[1], Shuang Song[2], Lu Zhang[2], Yunkun Dang[2,*] and Qun He[1,*]

[1]State Key Laboratory of Agrobiotechnology and MOA Key Laboratory of Soil Microbiology, College of Biological Sciences, China Agricultural University, Beijing 100193, China and [2]State Key Laboratory for Conservation and Utilization of Bio-Resources and Center for Life Science, School of Life Sciences, Yunnan University, Kunming, Yunnan 650091, China

Received July 24, 2021; Revised March 10, 2022; Editorial Decision March 13, 2022; Accepted March 15, 2022

ABSTRACT

Crucial mechanisms are required to restrict self-propagating heterochromatin spreading within defined boundaries and prevent euchromatic gene silencing. In the filamentous fungus *Neurospora crassa*, the JmjC domain protein DNA METHYLATION MODULATOR-1 (DMM-1) prevents aberrant spreading of heterochromatin, but the molecular details remain unknown. Here, we revealed that DMM-1 is highly enriched in a well-defined 5-kb heterochromatin domain upstream of the *cat-3* gene, hereby called *5H-cat-3* domain, to constrain aberrant heterochromatin spreading. Interestingly, aberrant spreading of the *5H-cat-3* domain observed in the *dmm-1*^{KO} strain is accompanied by robust deposition of histone variant H2A.Z, and deletion of *H2A.Z* abolishes aberrant spreading of the *5H-cat-3* domain into adjacent euchromatin. Furthermore, lysine 56 of histone H3 is deacetylated at the expanded heterochromatin regions, and mimicking H3K56 acetylation with an *H3K56Q* mutation effectively blocks H2A.Z-mediated aberrant spreading of the *5H-cat-3* domain. Importantly, genome-wide analyses demonstrated the general roles of H3K56 deacetylation and H2A.Z deposition in aberrant spreading of heterochromatin. Together, our results illustrate a previously unappreciated regulatory process that mediates aberrant heterochromatin spreading.

INTRODUCTION

In eukaryotes, genomic DNA associates with histones and non-histone proteins to form chromatin structures. Based on the degree of compaction, chromatin is categorized as euchromatin or heterochromatin. Heterochromatin is typically highly compacted at repetitive DNA regions to silence invasive transposons, which is critical for genome stability and organism viability (1,2). However, heterochromatin always poses a threat to adjacent euchromatin owing to its intrinsic spreading potential. The classical example is the position effect variegation (PEV) in *Drosophila melanogaster*, where chromosome rearrangement juxtaposes the *white* gene with pericentric heterochromatin. Consequently, the *white* gene is stochastically silenced in a portion of cells due to varying distances of heterochromatin spreading, resulting in mottled eyes (3,4). Heterochromatin disorders have been shown to be linked with many diseases, including carcinogenesis (5–7). Thus, eukaryotic genomes must establish boundaries to protect euchromatin from heterochromatin invasion (8,9).

The intrinsic spreading potential of heterochromatin is generally driven by the self-propagation of heterochromatin-associated histone modifications and chromatin proteins (10,11). In budding yeast, heterochromatin spreading depends on the positive feedback loop of H4K16 deacetylation and subsequent binding of SIR complex (Sir2/Sir3/Sir4) to deacetylated histones (10,12). Sir2/Sir4 deacetylates H4K16 at the nucleation sites, which increases the affinity of Sir3 to chromatin. Sir3 in turn recruits Sir2/Sir4 to deacetylate H4K16 in the adjacent nucleosomes and facilitates the spreading of entire Sir complex outwards from its nucleation sites (13). However, the self-propagation of Sir complex mediated-H4K16 deacetylation is not sufficient for silencing. Silencing occurs when Sir2 deacetylates H3K56 to close the nucleosomal entry-exit gates which enables compaction of heterochromatin (14). Given the strong effect of H3K56 acetylation (H3K56ac) on silencing, it is appealing to dissect the role of H3K56ac in organisms which use the H3K9 methylation (H3K9me)/HP1 system to assemble heterochromatin. Several mechanisms are exploited to prevent inappropriate spreading of heterochromatin in budding yeast, such as

*To whom correspondence should be addressed. Tel: +86 10 62731206; Fax: +86 10 62731206; Email: qunhe@cau.edu.cn
Correspondence may also be addressed to Yunkun Dang. Tel: +86 871 65931221; Email: ykdang@ynu.edu.cn

boundary elements (15–18) and competition between opposing histone modifications (19,20). Interestingly, histone variant H2A.Z/Htz1-incorporated nucleosomes can define the boundaries of heterochromatin domains to directly antagonize aberrant spreading of silent heterochromatin (21). However, the role of H2A.Z in regulating heterochromatin spreading outside of budding yeast remains unknown.

Neurospora crassa is a simple yet powerful model organism since it harbors the complete set of heterochromatic modifications conserved in higher eukaryotes, such as DNA methylation, making it ideal for studying the processes involved in heterochromatin formation (22). Unlike that in budding yeast, heterochromatin spreading in *N. crassa* is dominated by the H3K9me/HP1 system. Constitutive heterochromatin is mainly established at the relics of a genome defense system called repeat-induced point mutation (RIP), which are characterized by high AT-richness (23). The AT-rich cis-acting signal recruits the histone methyltransferase DIM-5 complex (DCDC) through an unknown mechanism, leading to H3K9 trimethylation (H3K9me3) (24–27). HP1 binds to H3K9me3 through its chromodomain and acts as a platform to recruit DNA methyltransferase DIM-2 which methylates cytosine residues within the AT-rich sequences (28–30). Once nucleated, heterochromatin spreading is initiated. Histone demethylase LSD1 is crucial for maintaining proper heterochromatin boundaries in *N. crassa* (31). In addition, DNA Methylation Modulator 1 (DMM-1), a JmjC domain protein, is preferentially localized to the edges of some heterochromatin domains in an HP1-dependent manner, where it antagonizes aberrant heterochromatin spreading (32). Similarly in fission yeast, the JmjC domain protein, Epe1, is recruited to the borders of heterochromatin in a Swi6/HP1-dependent manner and exerts proper boundary function (33,34). Although JmjC domain proteins are generally involved in histone demethylation, neither DMM-1 nor Epe1 possesses such activity (32,35). A study showed that Epe1 could recruit downstream effector Bdf2 to antagonize H4K16 deacetylation-mediated heterochromatin spreading (36). However, the mechanism by which DMM-1 blocks heterochromatin spreading is largely unknown.

We previously identified a 5-kb heterochromatin domain (*5H-cat-3* domain) which negatively regulates the expression levels of its proximal NCU00354 and NCU00355 (*cat-3*) genes in *N. crassa* (37). In addition, the histone variant H2A.Z, a negative regulator of *cat-3* expression, was enriched in both *cat-3* gene locus and the boundaries of the *5H-cat-3* domain (38). In this study, we demonstrated that DMM-1 is highly enriched in the *5H-cat-3* domain and restricts heterochromatin spreading mediated by H3K56 deacetylation and H2A.Z deposition. Importantly, genome-wide analyses further confirmed the general role of H3K56 deacetylation and H2A.Z deposition in regulating aberrant heterochromatin spreading. Our results uncovered a critical chromatin regulatory process that mediates aberrant spreading of heterochromatin.

MATERIALS AND METHODS

Strains and culture conditions

In this study, the *N. crassa 87–3* (*bd*, *a*) strain with *bd* mutation (*ras-1*^{T79I}) was used as the wild-type strain (39). The *ku70*^{RIP} (*bd*, *a*) strain in which the *ku70* ORF was mutated with multiple premature stop codons by repeat-induced point mutation (40) was used as the host strain for creating the knockout strains (*dmm-1*^{KO}) and knock-in strains (*dmm-1*$^{C\text{-}FLAG}$, *H3K56Q* and *H3K56R*), because the *ku70*^{RIP} strain with loss-of-function of Ku70 protein exhibits high homologous recombination efficiency and low non-homologous end-joining rate. The *cat-3*^{KO}, *hpo*^{KO} and *H2A.Z*^{KO} strains generated previously were also used in this study (26,27,37,38,41). The newly generated double mutants were *dmm-1*^{KO} *H2A.Z*^{KO}, *dmm-1*^{KO} *H3K56Q* and *dmm-1*^{KO} *H3K56R*. The *dmm-1*^{KO}, FLAG-DMM-1 strain was constructed by introducing pccg-1-3FLAG-DMM-1 plasmid into the *dmm-1*^{KO} host strain. All strains used here possess the same *bd* background.

Conidia of indicated strains were inoculated in petri dishes with 50 mL minimal medium (1 × Vogel's and 2% glucose) and cultured at 25°C in constant light until the exponential growth phase of mycelia. The mycelial mats were cut with a specific puncher for quantification. Then, these small mycelial disks were transferred to Erlenmeyer flasks with 50 mL minimal medium and were grown at 25°C with shaking for 18 hours under constant light.

Generation of antiserum against DMM-1

The GST-DMM-1 (amino acids Pro104-Asp396) fusion protein was expressed in *Escherichia coli* BL21 cells, and the soluble recombinant protein was purified and used as the antigen to generate rabbit polyclonal antiserum as previously described (26).

Protein analysis

Sample preparation, protein extraction and quantification as well as western blot analysis were performed as previously described (38). Equal amounts of total protein (32 μg) were loaded into each protein lane of SDS-polyacrylamide gel and separated by electrophoresis. Then, the total proteins were transferred onto PVDF membrane and western blot analysis was performed using antibody against the target protein.

In-gel assay for catalase activities

Sample preparation, protein extraction and quantification for the in-gel assay were same as previously described (37,38). Equal amounts of total protein (30 μg) were loaded into each protein lane of 7.5% native polyacrylamide gel. After 3 h electrophoresis, the gel was soaked in 7 mM H_2O_2 with gently shaking for 10 min, and then immediately transferred into a freshly prepared mixture containing 1% potassium hexacyanoferrate (III) and 1% iron (III) chloride hexahydrate. Catalase activities were visualized as the bright bands where H_2O_2 was decomposed by catalases.

RT-qPCR

Total RNA was extracted with TRIzol agent and treated with DNaseI to digest genomic DNA. Each RNA sample (5 μg) was subjected to reverse transcription with Maxima H Minus reverse transcriptase (Thermo Fisher Scientific #M1682), and then amplified by real-time qPCR (7500;

ABI). The primers used for RT-qPCR were shown in Supplementary Table S1. The relative value of gene expression was calculated using the $2^{-\Delta\Delta CT}$ method by comparing the cycle number for each sample to that for the untreated control (42). The results were normalized by the expression level of *β-tubulin* gene.

ChIP-qPCR

Chromatin immunoprecipitation (ChIP) assays were performed as previously described (41). Briefly, tissues were fixed with 1% formaldehyde for 15 min, and then treated with 125 mM glycine for 5 min to stop the cross-linking reaction. After harvest, cross-linked tissues were grinded (0.5 g) and re-suspended in 6 ml lysis buffer containing protease inhibitors. Chromatin was sheared by sonication to ∼500 bp fragments. 1 ml (2 mg/ml) protein was used as per immunoprecipitation and 10 μl was kept as the input DNA. ChIP was performed with 6 μl antibody to FLAG (Sigma), 10 μl antibody to HP1, 10 μl antibody to H2A.Z, 3 μl antibody to acetylated H3K56 (ab76307; Abcam) or 3 μl antibody to H3 (2650; CST). Immunoprecipitated DNA was enriched with the GammaBind G Sepharose beads (17-0885-02; GE Healthcare) and eluted using elution buffer. Finally, purified DNA was quantified by real-time qPCR (7500; ABI) with AceQ® Universal SYBR qPCR Master Mix (Q511; Vazyme) and primer pairs (see Supplementary Table S2). Occupancies were normalized by the input DNA and presented as a percentage of input DNA. H3K56 acetylation data need to be further normalized to histone H3 level.

ChIP-seq and data analyses

ChIP-seq samples were prepared as above described. DNA purity and concentration were measured using the NanoPhotometer® spectrophotometer (Implen) and Qubit® DNA Assay Kit in Qubit® 3.0 Flurometer (Life Technologies), respectively. Library construction was performed by Novogene Corporation (Beijing, China), and pair-end sequencing was performed on Illumina NovaSeq6000 platform. Raw reads that pass quality control were processed with Trim Galore (version 3.2) and mapped to *N. crassa* OR74A (NC10) genome using Bowtie2 (version 2.3.5.1) (43). Only unique mappers were retained for downstream analyses. Peak calling was performed using MACS2 (version 2.2.7.1) (44). Mapped read density was calculated over 10 bp bins and normalized by RPGC using bamCoverage from deepTools (version3.5.1) (45), denoised with sliding window (window size is 100 nt and step is 10 nt) and visualized with the Integrative Genomics Viewer (IGV) (46). The pipeline with detailed settings is available on GitHub (https://github.com/asuang/research-for-heterochromatin-in-NC).

Bisulfite-seq and data analyses

Bisulfite-sequencing sample preparation was performed using the MGIEasy WGBS Library Prep Kit (1000005251; MGI) for DNBSEQ™ platform (MGI) and the EZ DNA Methylation-Gold Kit (Zymo Research). Raw reads that pass quality control were performed with Bismark software (version 0.23.1) for alignment and quantification (47). Clean reads were mapped to *N. crassa* OR74A (NC10) genome using Bowtie2 (version 2.4.4) (43). Only unique mappers were retained for downstream analyses. The position and density of 5mC was evaluated by Bismark software with command bismark_methylation_extractor and visualized with the Integrative Genomics Viewer (IGV) (46). The pipeline for WGBS data processing, quantification and visualization are available on GitHub (https://github.com/asuang/research-for-heterochromatin-in-NC).

RESULTS

DMM-1 is required for the transcriptional activation of *cat-3* and NCU00354 genes by blocking aberrant heterochromatin spreading

To dissect the molecular details of aberrant heterochromatin spreading in *N. crassa*, we deleted the gene encoding DMM-1 (NCU01554) from the *ras-1^{bd}* wild-type (WT) background strain. As reported previously (32), the *dmm-1^{KO}* mutant showed a severe deficiency in conidial development on slants and a dramatic reduction of growth rate on plates (Figure 1A). Since HP1 protein is enriched in a 5-kb heterochromatin domain upstream of *cat-3* gene (*5H-cat-3* domain) and DMM-1 has been shown to localize to the boundaries of some heterochromatin domains in an HP1-dependent manner (32,37), we generated a *dmm-1$^{C\text{-}FLAG}$* knock-in strain and performed ChIP assay to determine the binding profile of DMM-1-FLAG at the *5H-cat-3* domain. Anti-FLAG antibody and oligonucleotide primer pairs (primer pairs from -3 to 6) designed to target the *5H-cat-3* domain and its adjacent regions were used in the ChIP assay (Figure 1B). The results showed that DMM-1-FLAG was highly enriched in the middle region of the *5H-cat-3* domain (primer pairs 2 and 4) and its boundaries (primer pairs 1 and 5) (Figure 1C). The binding profile of DMM-1 at the *5H-cat-3* domain is similar to that of HP1, as previously shown (37). To further confirm the enrichment of DMM-1 at the *5H-cat-3* domain, we generated antiserum specifically against DMM-1 (Figure 1D) and performed ChIP assay using the DMM-1 antibody. As expected, DMM-1 was highly enriched in the middle region of the *5H-cat-3* domain (primer pairs 2 and 4) and its boundaries (primer pairs 1 and 5) in the WT strain but not in the *dmm-1^{KO}* strain (Figure 1E).

To determine whether DMM-1 functions at the *5H-cat-3* domain, we used an HP1-specific antibody to perform ChIP assays that cover a 10-kb chromatin region from the 3′UTR of NCU00353 to the transcription start site (TSS) of *cat-3* (Figure 1B). In the WT strain, HP1 was specifically enriched in the *5H-cat-3* domain (primer pairs from 1 to 5). In the *dmm-1^{KO}* strain, however, HP1 enrichment was significantly increased at adjacent euchromatin regions including the *cat-3* promoter (primer pairs 5), NCU00354 gene locus (primer pairs −3) and the intergenic region between NCU00353 and NCU00354 loci (primer pairs −6 and −4) compared to those in the WT strain (Figure 1F). These results indicate that HP1 aberrantly spreads from the *5H-cat-3* domain into adjacent euchromatin regions in the *dmm-1^{KO}* strain. Consistently, whole genome bisulfite sequencing (WGBS) results confirmed that DNA methylation also aberrantly spread from the *5H-cat-3* domain into the *cat-3*

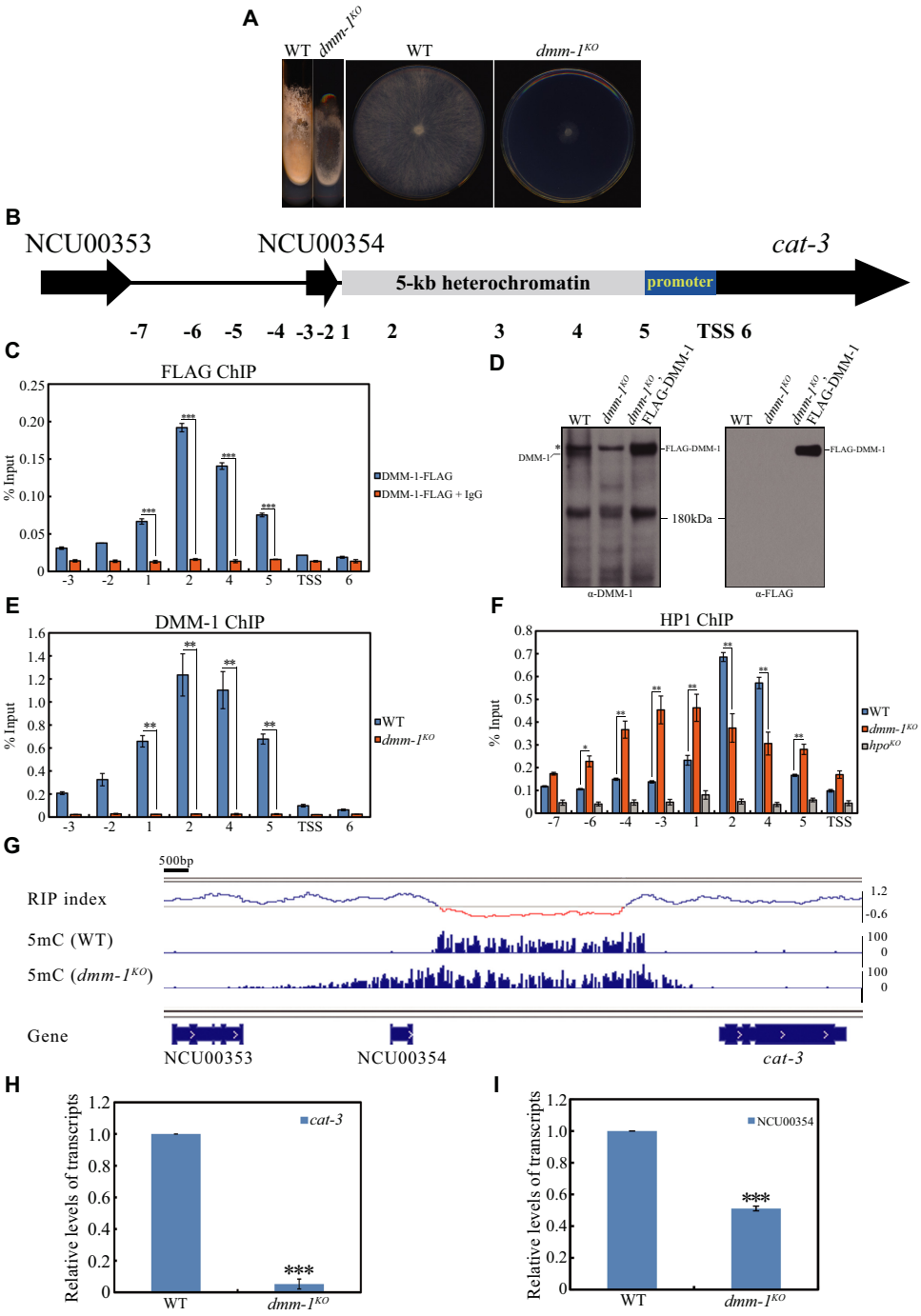

Figure 1. DMM-1 is required for transcriptional activation of *cat-3* and NCU00354 genes by blocking aberrant heterochromatin spreading. (**A**) Growth phenotypes of the wild-type (WT) and *dmm-1*^{KO} strains on slants and plates, respectively. (**B**) Schematic diagram depicting a 5-kb heterochromatin domain (*5H-cat-3* domain) located between *cat-3* (NCU00355) and NCU00354 genes on linkage group III of the *N. crassa* genome. Primer pairs from −7 to 6 under the schematic diagram indicate regions tested by ChIP-qPCR. TSS, transcription start site. (**C**) ChIP assay with the FLAG antibody showing the binding pattern of DMM-1-FLAG at the *5H-cat-3* domain and its adjacent regions in the *dmm-1*$^{C\text{-}FLAG}$ strain. IgG, immunoglobulin G. Error bars indicate S.D. ($n = 3$). ***$P < 0.001$. Unpaired Student's *t* test was used. (**D**) Immunodetection of DMM-1 in the WT, *dmm-1*^{KO} mutant and *dmm-1*^{KO}, FLAG-DMM-1 transformant using polyclonal antiserum that specifically recognizes endogenous DMM-1 protein in the WT strain and the ectopically expressed FLAG-DMM-1 in the transformant strain. Asterisk indicates non-specific band. (**E**) ChIP assay using the DMM-1 antibody showing the enrichment profile of DMM-1 at the *5H-cat-3* domain and its adjacent regions in the WT strain. The *dmm-1*^{KO} strain was used as the negative control. Error bars indicate S.D. ($n = 3$). **P < 0.01. Unpaired student's t test was used. (**F**) ChIP assay with the HP1 antibody showing the binding pattern of HP1 at the *5H-cat-3* domain and its adjacent regions in the WT and *dmm-1*^{KO} strains. The *hpo*^{KO} strain was used as the negative control. Error bars indicate S.D. ($n = 3$). *$P < 0.05$; **$P < 0.01$. Unpaired student's t test was used. (**G**) WGBS tracks displaying the distribution of DNA methylation in the WT and *dmm-1*^{KO} strains over the *5H-cat-3* domain and its adjacent regions. The horizontal line in the RIP index panel indicates the threshold (<0.7) to trigger DNA methylation by RIP (52). Red region represents the *5H-cat-3* domain. (**H** and **I**) RT-qPCR assay showing the mRNA levels of *cat-3* (H) and NCU00354 (I) in the WT and *dmm-1*^{KO} strains, respectively. Error bars indicate S.D. ($n = 3$). ***$P < 0.001$. Unpaired Student's *t* test was used.

promoter, NCU00354 locus and the intergenic region between NCU00354 and NCU00353 in the *dmm-1*^{KO} strain (Figure 1G), which is consistent with the spreading profile of HP1.

Consequently, the levels of *cat-3* and NCU00354 mRNA (Figure 1H and I), CAT-3 activity (Supplementary Figure S1A) as well as CAT-3 protein (Supplementary Figure S1B) in the *dmm-1*^{KO} strain were significantly decreased compared to those in the WT strain, further confirming the encroachment of the *5H-cat-3* domain on adjacent euchromatic genes. Together, these results demonstrate that DMM-1 is required for maintaining normal transcription of *cat-3* and NCU00354 genes by preventing aberrant spreading of the *5H-cat-3* domain.

Aberrant heterochromatin spreading is associated with H2A.Z deposition in the *dmm-1*^{KO} strain

We previously showed that the boundaries of the *5H-cat-3* domain and the *cat-3* gene locus were enriched with histone variant H2A.Z, and the deposition of H2A.Z at the *cat-3* promoter and TSS played a suppressive role in *cat-3* expression (38). In budding yeast, deposition of H2A.Z near the telomeres or the silent *HMR* mating-type locus could protect euchromatin from gene silencing caused by heterochromatin spreading (21). To determine whether the deposition of H2A.Z at the boundaries of the *5H-cat-3* domain functions like that in budding yeast, we examined the enrichment of HP1 around the *5H-cat-3* domain in the WT and *H2A.Z*^{KO} strains. ChIP results showed that although HP1 enrichment at the middle region of the *5H-cat-3* domain (primer pairs 2 and 4) was increased, H2A.Z deletion did not cause HP1 to spread outside of the boundaries (primer pairs 1 and 5) (Figure 2A). Similar to the binding pattern of HP1, DMM-1 enrichment at the middle region of the *5H-cat-3* domain (primer pairs 2 and 4) was also increased in the *H2A.Z*^{KO} strain (Figure 2B). Moreover, loss of H2A.Z led to elevated enrichment of DMM-1 at the *5H-cat-3* domain boundaries compared to those in the WT strain (Figure 2B), suggesting that DMM-1 enrichment at the boundaries may depend on other factors other than HP1, which are inhibited by H2A.Z deposition. Taken together, these results strongly suggest that H2A.Z negatively influences the association of HP1 and DMM-1 at the *5H-cat-3* domain but is not required for defining the heterochromatin boundary as it does in budding yeast.

To further explore the role of H2A.Z deposition at the *5H-cat-3* domain boundaries, we measured the occupancy of H2A.Z around the *5H-cat-3* domain in the *dmm-1*^{KO} strain. Unexpectedly, we found that H2A.Z enrichment was dramatically increased from the 3′UTR of NCU00353 to the *cat-3* promoter region in the *dmm-1*^{KO} strain compared to those in the WT strain (Figure 2C), similar to the spreading pattern of the *5H-cat-3* domain. ChIP sequencing data also further confirmed the highly elevated H2A.Z deposition around the *5H-cat-3* domain in the *dmm-1*^{KO} strain (Figure 2D). RT-qPCR and western blot analyses revealed that the levels of *H2A.Z* mRNA and H2A.Z protein were only slightly elevated in the *dmm-1*^{KO} mutant compared to those in the WT strain (Supplementary Figure S2A and B). To determine whether DMM-1 only affects the deposition of H2A.Z around heterochromatin domains in the *dmm-1*^{KO} strain, we checked the enrichment of H2A.Z at the promoter region of *eed* gene (NCU05300), which is a known H2A.Z-enriched euchromatic locus (48). ChIP result showed that loss of DMM-1 had no effect on H2A.Z deposition at the *eed* promoter region (Figure 2E). We further performed ChIP sequencing to verify this pattern. As shown in Figure 2F, DMM-1 deletion did not affect H2A.Z deposition at the euchromatin regions from NCU05305 gene to NCU05286 gene. These data indicate that the impact of DMM-1 deletion on H2A.Z localization may be specific for heterochromatic flanks. Thus, sharp deposition of H2A.Z accompanied by aberrant heterochromatin spreading may be caused by aberrant incorporation or removal of H2A.Z on the chromatin rather than enhanced *H2A.Z* expression.

H2A.Z deposition is crucial for aberrant heterochromatin spreading in the *dmm-1*^{KO} strain

Sharp deposition of H2A.Z on the spreading path prompted us to investigate the role of H2A.Z in heterochromatin spreading caused by DMM-1 deletion. To this end, we generated a *dmm-1*^{KO} *H2A.Z*^{KO} double mutant. As illustrated in Figure 3A, the conidial development and growth rate of the *dmm-1*^{KO} *H2A.Z*^{KO} double mutant resembled those of the *H2A.Z*^{KO} single mutant, which were healthier than those of the *dmm-1*^{KO} single mutant. Likewise, the low levels of *cat-3* and NCU00354 mRNA (Figure 3B and C), CAT-3 activity (Supplementary Figure S3A) as well as CAT-3 protein (Supplementary Figure S3B) observed in the *dmm-1*^{KO} strains were all dramatically elevated in the *dmm-1*^{KO} *H2A.Z*^{KO} strain, comparable to those in the *H2A.Z*^{KO} single mutant but higher than those in the WT strain. These results imply that H2A.Z deposition is crucial for aberrant spreading of heterochromatin caused by DMM-1 deletion.

To test this possibility, we measured HP1 enrichment around the *5H-cat-3* domain in the WT, *dmm-1*^{KO}, *H2A.Z*^{KO} and *dmm-1*^{KO} *H2A.Z*^{KO} strains. As shown in Figure 3D, aberrant spreading of HP1 towards adjacent euchromatin regions in the *dmm-1*^{KO} mutant disappeared and the enrichment peaks of HP1 were strongly constricted to the *5H-cat-3* domain (primer pairs from 1 to 5) in the *dmm-1*^{KO} *H2A.Z*^{KO} strain, suggesting that aberrant spreading of HP1 depends on H2A.Z deposition. Similarly, aberrant spreading of DNA methylation towards adjacent euchromatin regions in the *dmm-1*^{KO} mutant was strictly restricted within the *5H-cat-3* domain in the *dmm-1*^{KO} *H2A.Z*^{KO} strain (Figure 3E), indicating that H2A.Z-dependent HP1 enrichment drives aberrant spreading of DNA methylation into euchromatin regions. Taken together, these results demonstrate that H2A.Z deposition is crucial for aberrant spreading of heterochromatin caused by DMM-1 deletion.

H3K56 deacetylation is required for H2A.Z-mediated aberrant heterochromatin spreading in the *dmm-1*^{KO} strain

Genome-wide analysis in yeast revealed widespread reduction of H2A.Z levels in mutants with hyperacetylated H3K56 (49). Moreover, the formation of silent heterochromatin was controlled by H3K56 deacetylation that promotes an inaccessible and silent chromatin structure

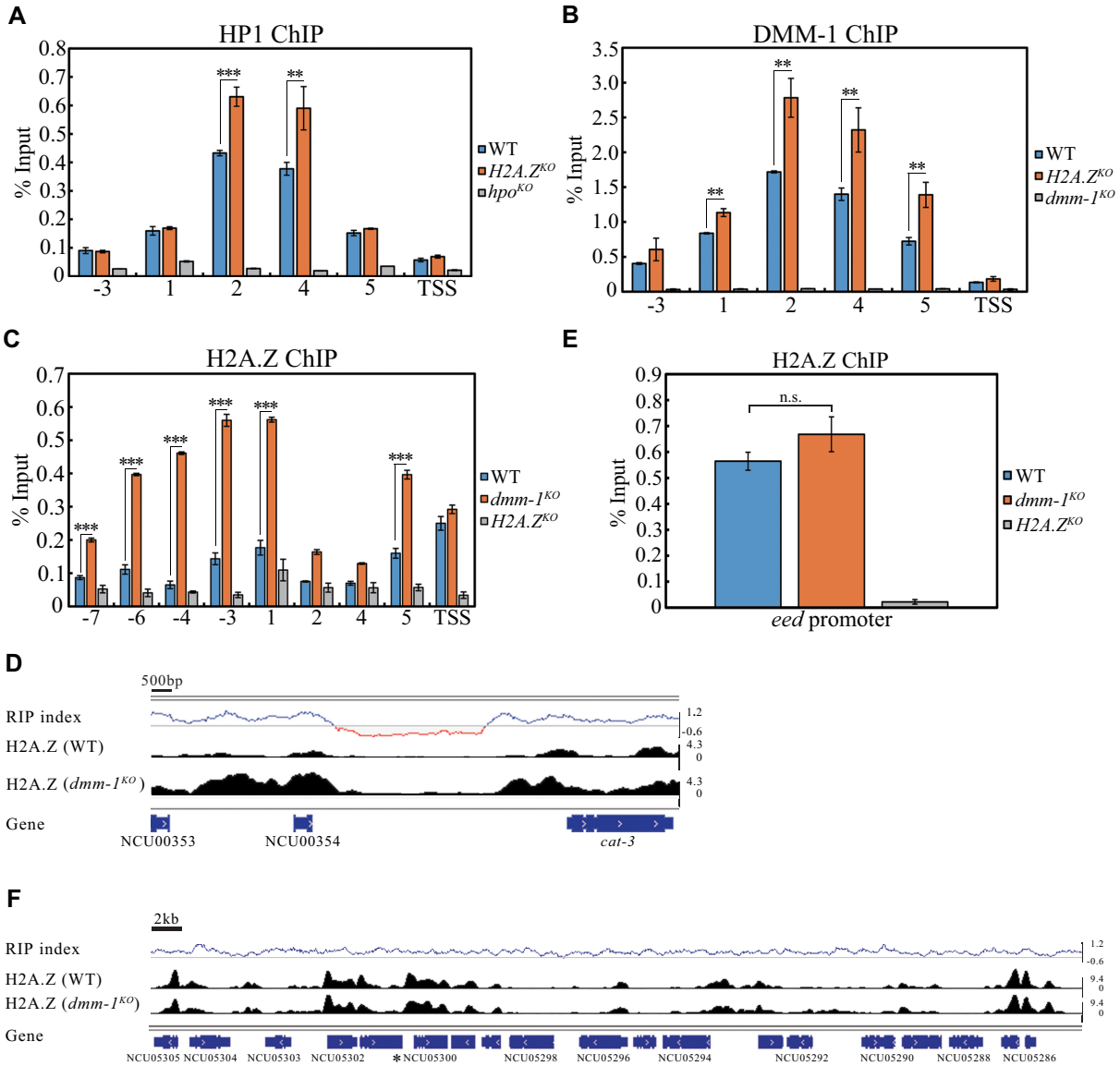

Figure 2. H2A.Z is sharply deposited on the spreading path of the *5H-cat-3* domain in the *dmm-1*^{KO} strain. (**A**) ChIP assay using the HP1 antibody showing the enrichment profile of HP1 at the *5H-cat-3* domain and its adjacent regions in the WT and *H2A.Z*^{KO} strains. The *hpo*^{KO} strain was used as the negative control. Error bars indicate S.D. ($n = 3$). $^{**}P < 0.01$; $^{***}P < 0.001$. Unpaired Student's *t* test was used. (**B**) ChIP assay using the DMM-1 antibody showing the enrichment profile of DMM-1 at the *5H-cat-3* domain and its adjacent regions in the WT and *H2A.Z*^{KO} strains. The *dmm-1*^{KO} strain was used as the negative control. Error bars indicate S.D. ($n = 3$). $^{**}P < 0.01$. Unpaired Student's *t* test was used. (**C**) ChIP assay using the H2A.Z antibody showing the enrichment profile of H2A.Z at the *5H-cat-3* domain and its adjacent regions in the WT and *dmm-1*^{KO} strains. The *H2A.Z*^{KO} strain was used as the negative control. Error bars indicate S.D. ($n = 3$). $^{***}P < 0.001$. Unpaired Student's *t* test was used. (**D**) ChIP-seq tracks showing H2A.Z enrichment around the *5H-cat-3* domain in the WT and *dmm-1*^{KO} strains. The horizontal line in the RIP index panel indicates the threshold (<0.7) to trigger DNA methylation by RIP. Red region represents the *5H-cat-3* domain. (**E**) ChIP assay using the H2A.Z antibody showing the enrichment profile of H2A.Z at the promoter region of *eed* gene in the WT and *dmm-1*^{KO} strains. The *H2A.Z*^{KO} strain was used as the negative control. Error bars indicate S.D. ($n = 3$). n.s., no significance. Unpaired Student's *t* test was used. (**F**) ChIP-seq tracks showing H2A.Z enrichment at the euchromatin regions from NCU05305 to NCU05286 in the WT and *dmm-1*^{KO} strains. The horizontal line in the RIP index panel indicates the threshold (<0.7) to trigger DNA methylation by RIP.

(14). To examine whether H3K56 acetylation is related to H2A.Z-mediated aberrant heterochromatin spreading, we measured H3K56 acetylation levels around the *5H-cat-3* domain in the WT and *dmm-1*^{KO} strains. ChIP results revealed that loss of DMM-1 down-regulated H3K56 acetylation at the corresponding H2A.Z deposition regions compared to those in the WT strain (Figure 4A), suggesting an antagonizing relationship between H3K56 acetylation and H2A.Z deposition at the flanks of *5H-cat-3* domain in the *dmm-1*^{KO} mutant. To further determine the role of H3K56 acetylation in H2A.Z-mediated aberrant heterochromatin spreading, we generated *H3K56R*, *dmm-1*^{KO} *H3K56R*, *H3K56Q* and *dmm-1*^{KO} *H3K56Q* mutants, in which the mutation of K56 to R abolishes H3K56 acetylation whereas the mutation of K56 to Q mimics H3K56 acetylation (50,51). As shown in Figure 4B, the *dmm-1*^{KO}

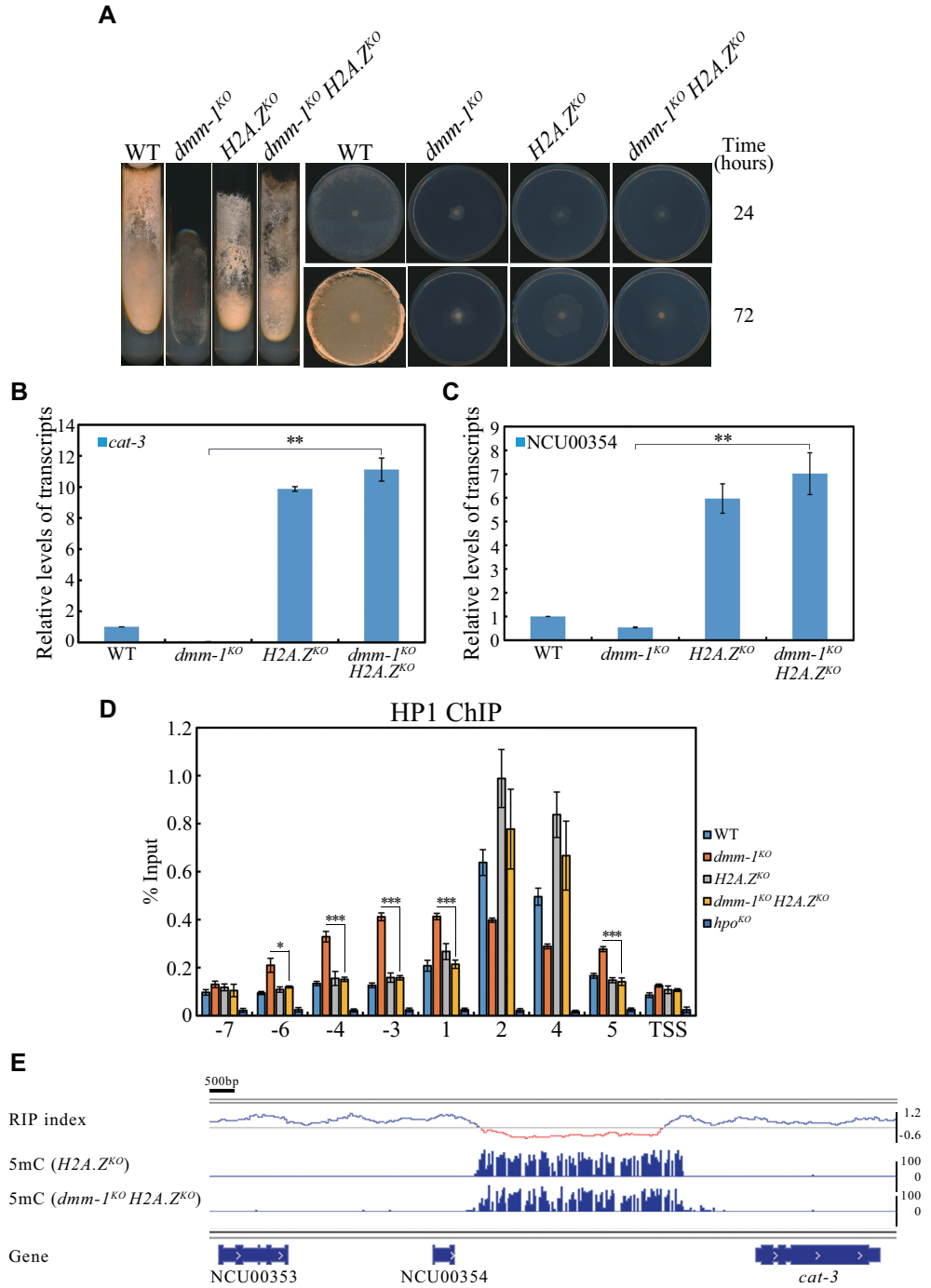

Figure 3. Loss of H2A.Z effectively blocks aberrant spreading of the *5H-cat-3* domain caused by DMM-1 deletion. (**A**) Growth phenotypes of the WT, *dmm-1*^{KO}, *H2A.Z*^{KO} and *dmm-1*^{KO} *H2A.Z*^{KO} strains on slants and plates, respectively. (**B** and **C**) RT-qPCR assays showing the mRNA levels of *cat-3* (B) and NCU00354 (C) in the WT, *dmm-1*^{KO}, *H2A.Z*^{KO} and *dmm-1*^{KO} *H2A.Z*^{KO} strains. Error bars indicate S.D. ($n = 3$). $^{**}P < 0.01$. Unpaired Student's *t* test was used. (**D**) ChIP assay using the HP1 antibody showing the enrichment profile of HP1 at the *5H-cat-3* domain and its adjacent regions in the WT, *dmm-1*^{KO}, *H2A.Z*^{KO} and *dmm-1*^{KO} *H2A.Z*^{KO} strains. The *hpo*^{KO} strain was used as the negative control. Error bars indicate S.D. ($n = 3$). $^{*}P < 0.05$; $^{***}P < 0.001$. Unpaired Student's *t* test was used. (**E**) WGBS tracks displaying the distribution of DNA methylation in the *H2A.Z*^{KO} and *dmm-1*^{KO} *H2A.Z*^{KO} strains over the *5H-cat-3* domain and its adjacent regions. The horizontal line in the RIP index panel indicates the threshold (<0.7) to trigger DNA methylation by RIP. Red region represents the *5H-cat-3* domain.

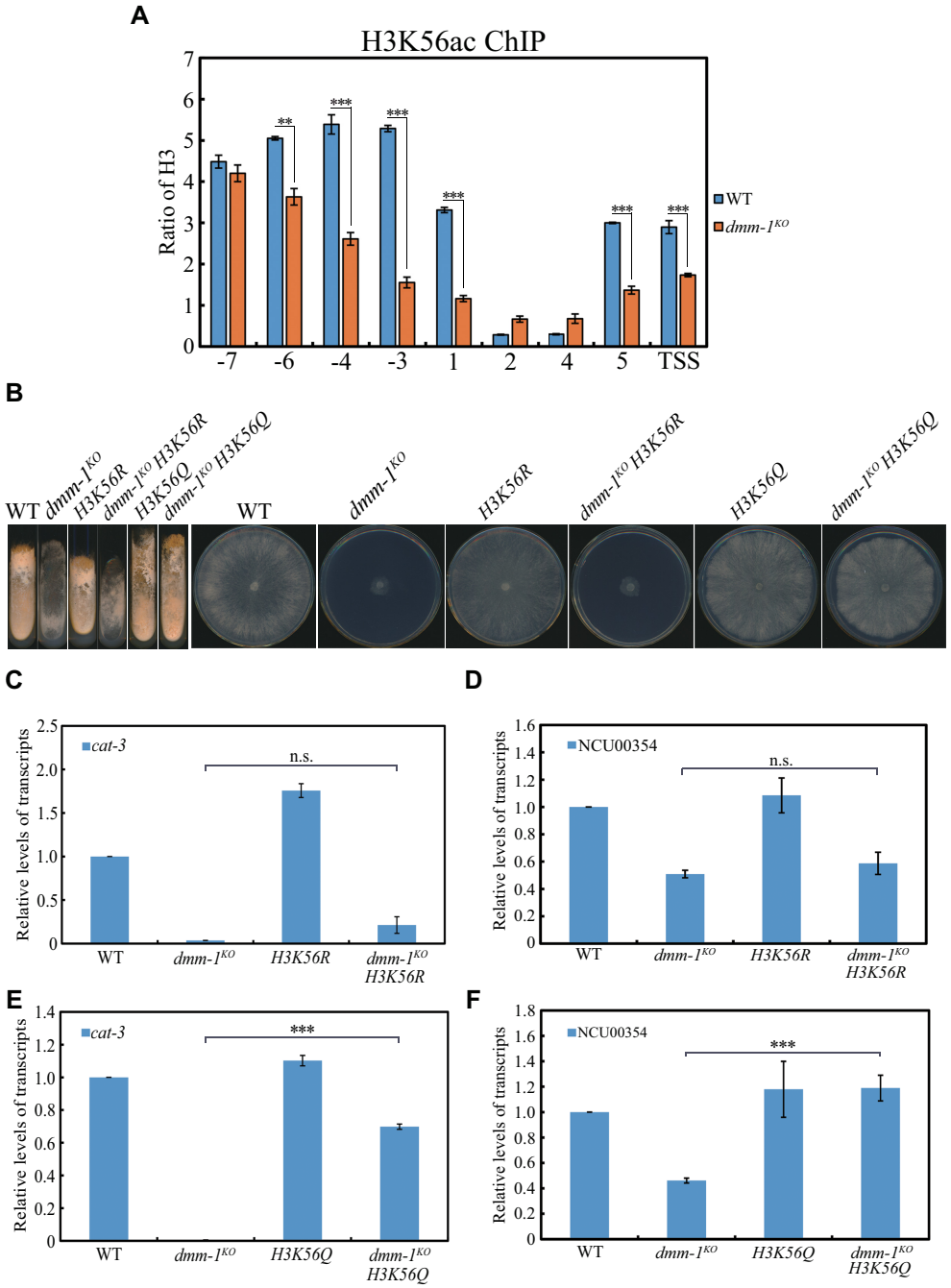

Figure 4. Mimicking H3K56ac by an *H3K56Q* mutation rescues the growth defect and the repression of *cat-3* and NCU00354 genes in the *dmm-1*^{KO} mutant. (**A**) ChIP assay showing the relative enrichment of H3K56ac at the *5H-cat-3* domain and its adjacent regions in the WT and *dmm-1*^{KO} strains. The relative enrichment of H3K56ac represented the ratio of H3K56ac to H3. Error bars indicate S.D. ($n = 3$). $^{**}P < 0.01$; $^{***}P < 0.001$. Unpaired Student's *t* test was used. (**B**) Growth phenotypes of the WT, *dmm-1*^{KO}, *H3K56R*, *dmm-1*^{KO} *H3K56R*, *H3K56Q* and *dmm-1*^{KO} *H3K56Q* strains on slants and plates, respectively. (**C**–**F**) RT-qPCR assays showing the mRNA levels of *cat-3* and NCU00354 in the WT, *dmm-1*^{KO}, *H3K56R* and *dmm-1*^{KO} *H3K56R* strains (C and D) or WT, *dmm-1*^{KO}, *H3K56Q* and *dmm-1*^{KO} *H3K56Q* strains (E and F). Error bars indicate S.D. ($n = 3$). $^{***}P < 0.001$. n.s., no significance. Unpaired Student's *t* test was used.

H3K56R double mutant phenocopied the *dmm-1^{KO}* strain, while the *dmm-1^{KO} H3K56Q* double mutant resembled the WT strain and *H3K56Q* single mutant. Consistent with the growth phenotypes, the levels of *cat-3* and NCU00354 mRNA, CAT-3 activity as well as CAT-3 protein remained repressed in the *dmm-1^{KO} H3K56R* double mutant (Figure 4C, D, Supplementary Figure S4A and B) but were almost restored to the levels of the WT strain in the *dmm-1^{KO} H3K56Q* double mutant (Figure 4E, F, Supplementary Figure S4C and D). These results demonstrate that H3K56 deacetylation is required for H2A.Z-mediated aberrant heterochromatin spreading in the *dmm-1^{KO}* mutant.

As expected, the enrichment profiles of H2A.Z and HP1 around the *5H-cat-3* domain in the *dmm-1^{KO} H3K56Q* strain were similar to those of the WT and *H3K56Q* strains (Figure 5A and B), suggesting that H3K56 hyperacetylation blocks H2A.Z-mediated aberrant spreading of HP1 towards adjacent euchromatin regions in the *dmm-1^{KO}* mutant. However, abolishing H3K56 acetylation via *H3K56R* mutation could not restrict H2A.Z-mediated aberrant HP1 spreading caused by DMM-1 deletion (Figure 5C and D). WGBS also revealed that *H3K56Q*, but not *H3K56R*, prevented aberrant spreading of DNA methylation observed in the *dmm-1^{KO}* mutant (Figure 5E). Taken together, these results strongly suggest that H3K56 deacetylation is required for H2A.Z-mediated aberrant heterochromatin spreading in the *dmm-1^{KO}* strain.

Aberrant heterochromatin spreading mediated by H3K56 deacetylation and H2A.Z deposition occurs genome-widely in the *dmm-1^{KO}* strain

To determine whether aberrant heterochromatin spreading mediated by H3K56 deacetylation and H2A.Z deposition is a general mechanism, we performed and analyzed chromatin immunoprecipitation sequencing (ChIP-seq) and whole genome bisulfite sequencing (WGBS). Because the RIP process is tightly correlated with DNA methylation and heterochromatin formation, we used the DNA RIP index as an indicator to define the boundaries of methylated regions (52). To minimize the noise from RIP index, RIP relics <1.5 kb apart in the *N. crassa* genome were merged and 532 targeted regions were obtained. Furthermore, DMM-1-regulated RIP domains were defined as regions where HP1 and DNA methylation aberrantly spread for at least 1 kb from the boundaries of RIP relics into adjacent regions. Consequently, 137 of the 532 RIP domains were screened out for subsequent bioinformatics analysis, which is largely consistent with the proportion (17/45) of a previous study focused on Linkage Group VII (32). As shown in Figure 6, aberrant spreading of HP1 and DNA methylation outside of the boundaries were generally accompanied by H2A.Z incorporation and H3K56 deacetylation. More importantly, loss of H2A.Z or mimicking H3K56 acetylation via an *H3K56Q* mutation effectively restricted aberrant spreading of HP1 and DNA methylation in *N. crassa* genome (Figure 7). Data from 10 representative RIP regions were shown in Supplementary Figure S5. Together, these results suggest that aberrant heterochromatin spreading mediated by H3K56 deacetylation and H2A.Z deposition is a universal mechanism in the *dmm-1^{KO}* strain.

DISCUSSION

Unchecked heterochromatin can encroach on adjacent gene-rich euchromatin, causing euchromatic gene silencing. In *N. crassa*, DMM-1 is critical for setting heterochromatin boundaries and preventing aberrant spreading of heterochromatin. Here, we discovered that aberrant spreading of heterochromatin in the *dmm-1^{KO}* mutant is accompanied by H2A.Z deposition, and the enrichment profile is similar to those of HP1 and DNA methylation. Deletion of *H2A.Z* restricts HP1 and DNA methylation within heterochromatic regions, indicating that aberrant spreading of heterochromatin depends on H2A.Z deposition. Moreover, we demonstrated that the deacetylation of H3K56 is required for H2A.Z-dependent heterochromatin spreading, because *H3K56Q* mutation, which mimics hyperacetylation of H3K56, completely blocks aberrant heterochromatin spreading caused by DMM-1 deletion. Collectively, our results suggest that DMM-1 maintains the normal heterochromatin patterns by regulating H3K56 deacetylation and H2A.Z deposition (Figure 8).

The possible working model of DMM-1 in boundary formation

Although DMM-1 is only conserved in the filamentous fungi (32), functional parallels can be drawn to the well-characterized boundary protein Epe1 in fission yeast (33,34,36,53). Boundary elements containing specific DNA sequences serve as platforms for recruiting Epe1 to separate heterochromatin from euchromatin in fission yeast (2,33,34,36,53). However, sequence-specific boundary elements have not been identified in *N. crassa*. The specific localization of DMM-1 may be regulated by recognizing unknown DNA sequences or undefined chromatin marks via its cysteine-rich domains (32).

In fission yeast, histone deacetylase Sir2-mediated H4K16 deacetylation is crucial for heterochromatin spreading outside of the boundaries. To block the encroachment of heterochromatin on euchromatin, Bdf2 is enriched in the boundary elements through its interaction with Epe1, where it could protect acetylated H4 tails from deacetylation by Sir2 and therefore antagonize heterochromatin spreading (36). Similarly in *N. crassa*, the boundary effector LSD1 prevents aberrant heterochromatin spreading by suppressing HCHC complex-mediated histone deacetylation (31). While the requirement of HCHC activity for heterochromatin spreading in the *dmm-1^{KO}* mutant has not been verified, it is possible that DMM-1 recruits Bdf2-like factors to antagonize heterochromatin spreading mediated by H3K56 deacetylation.

Implications of H3K56 acetylation in heterochromatin structure

In budding yeast, Sir2-mediated H4K16 deacetylation has long been linked to Sir protein binding and subsequent spreading along silent loci (54). Consistent with this, histone acetyltransferase Sas2-mediated H4K16ac increases gradually from the telomere end to the adjacent euchromatic region and thus limits Sir protein spreading within silent re-

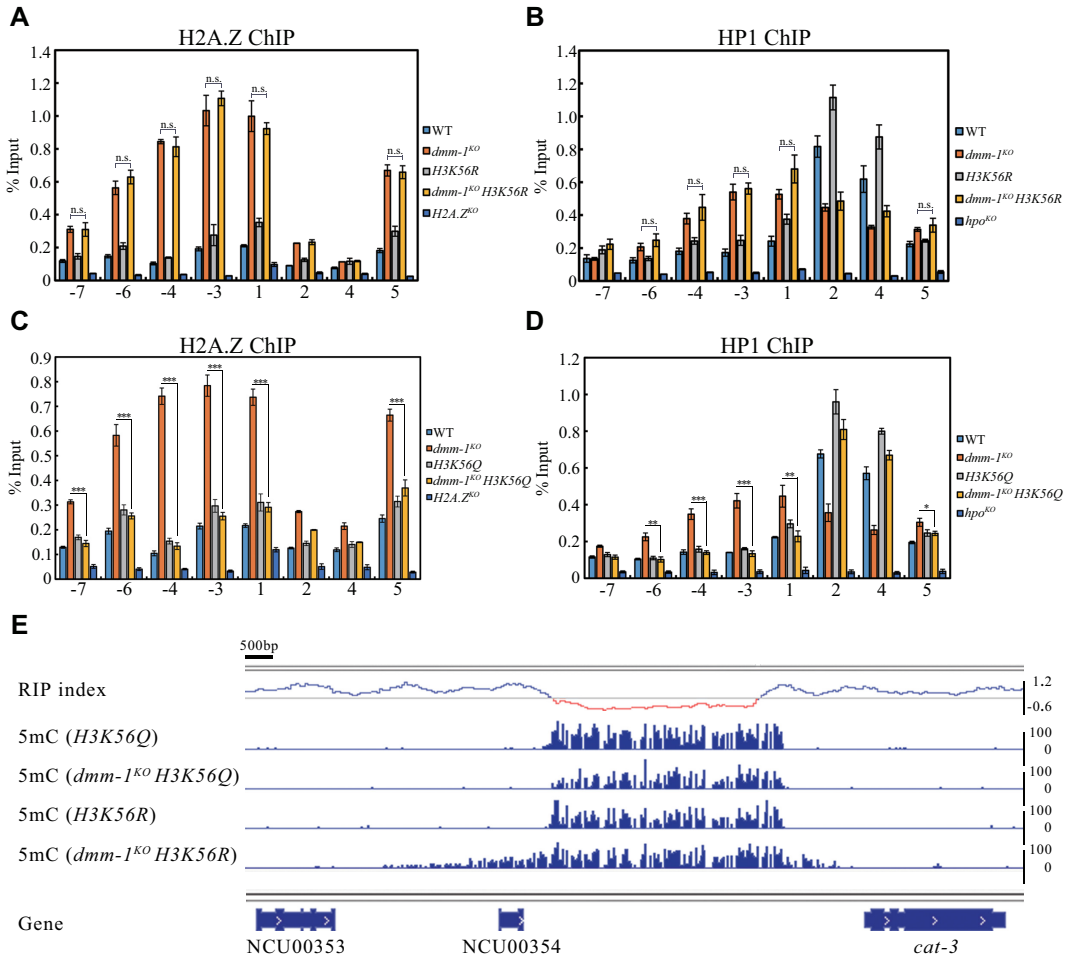

Figure 5. Mimicking H3K56ac by an *H3K56Q* mutation blocks the H2A.Z-dependent aberrant spreading of the *5H-cat-3* domain. (**A** and **B**) ChIP assays showing the binding patterns of H2A.Z (A) and HP1 (B) at the *5H-cat-3* domain and its adjacent regions in the WT, *dmm-1*^{KO}, *H3K56R* and *dmm-1*^{KO} *H3K56R* strains. The *H2A.Z*^{KO} and *hpo*^{KO} strains were used as the negative controls in (A) and (B), respectively. Error bars indicate S.D. ($n = 3$). n.s., no significance. Unpaired student's t test was used. (**C** and **D**) ChIP assays showing the binding patterns of H2A.Z (C) and HP1 (D) at the *5H-cat-3* domain and its adjacent regions in the WT, *dmm-1*^{KO}, *H3K56Q* and *dmm-1*^{KO} *H3K56Q* strains. The *H2A.Z*^{KO} and *hpo*^{KO} strains were used as the negative controls in (C) and (D), respectively. Error bars indicate S.D. ($n = 3$). *$P < 0.05$; **$P < 0.01$; ***$P<0.001$. Unpaired Student's *t* test was used. (**E**) WGBS tracks displaying the distribution of DNA methylation in *H3K56Q*, *dmm-1*^{KO} *H3K56Q*, *H3K56R* and *dmm-1*^{KO} *H3K56R* strains over the *5H-cat-3* domain and its adjacent regions. The horizontal line in the RIP index panel indicates the threshold (<0.7) to trigger DNA methylation by RIP. Red region represents the *5H-cat-3* domain.

gions (19,20). However, deacetylation of H4K16 alone is insufficient for silencing (55,56). Silencing requires deacetylation of H3K56 by Sir2, which promotes an inaccessible and silent chromatin structure (14). We showed here that lysine 56 of histone H3 is deacetylated at aberrant spreading path, and mimicking H3K56ac with an *H3K56Q* mutation prevents the encroachment of heterochromatin on adjacent euchromatin, indicating that H3K56 deacetylation is required for heterochromatin spreading outside of the boundaries in *N. crassa*. Although the implications of H3K56 acetylation in heterochromatin spreading have not been defined in other model organisms, it is possible and reasonable that the H3K56 acetylation levels serve as the deepest molecular switch to regulate the opening and condensing of chromatin structures because lysine 56 in H3 is located at the critical entry-exit points of the DNA superhelix surrounding the nucleosome (51). Furthermore, trimethylation of H3K56 has been defined as a conserved heterochromatic mark in mammalian cells (57). Therefore, it would be attractive to explore whether a transition from acetylation to methylation at the H3K56 residue regulates heterochromatin structure in mammals.

Interestingly, why does mimicking H3K56ac block aberrant heterochromatin spreading caused by DMM-1 deletion but does not disrupt the silencing of heterochromatin itself in the WT strain. Such a dichotomy may be attributed to the distinctive sequence feature of *N. crassa* heterochromatin because substantial AT-rich sequences created by RIP have been shown to recruit the DCDC complex to establish H3K9me3 and subsequent methylation of underlying DNA (58–60). However, the sharply decreasing AT-content at adjacent euchromatin regions is insufficient for DCDC-induced heterochromatin, hence heterochromatin spreading outside of the boundaries probably depends on histone deacetylation events, such as H3K56 deacetylation (31).

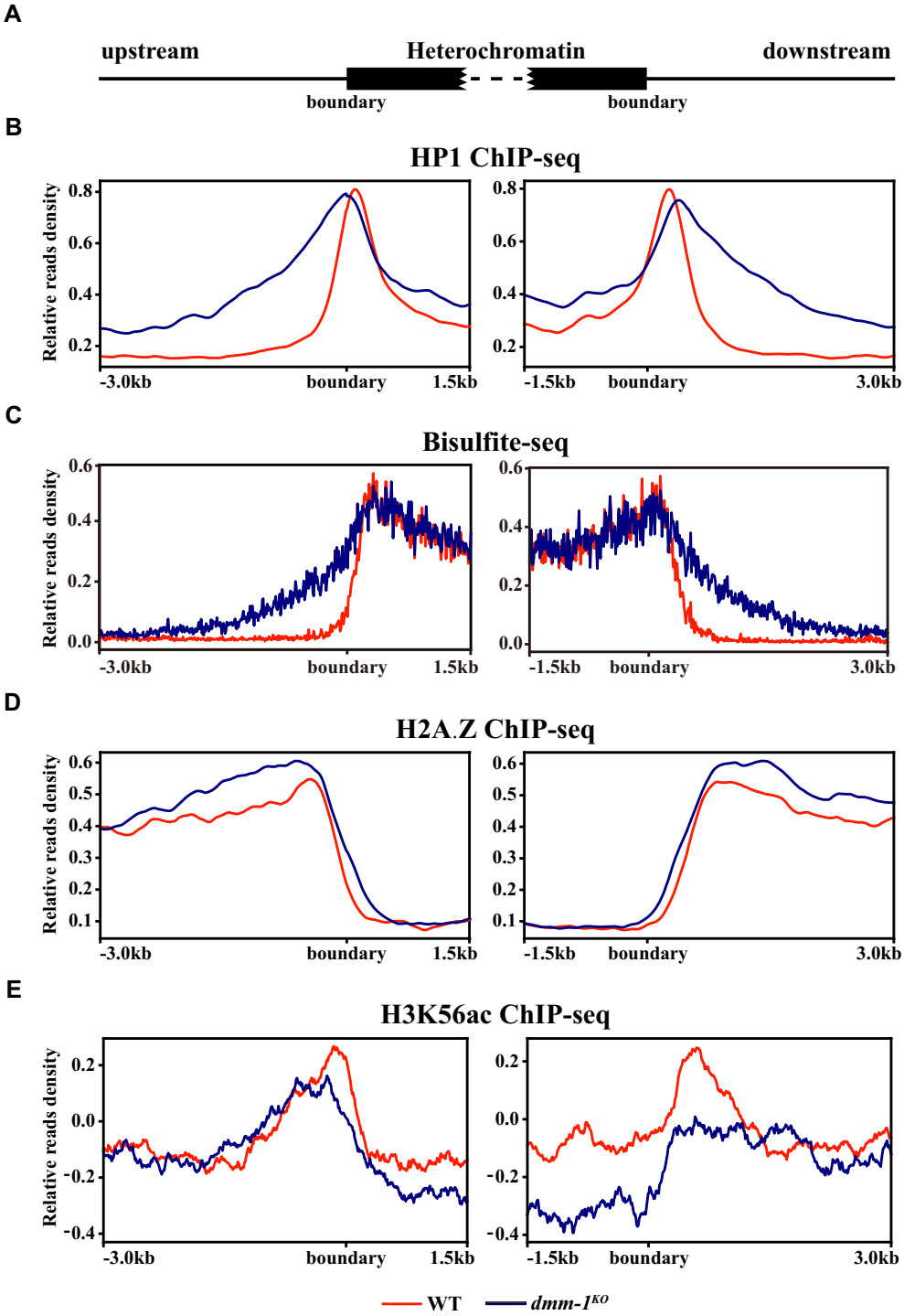

Figure 6. Aberrant heterochromatin spreading is generally accompanied by H2A.Z incorporation and H3K56 deacetylation in the *dmm-1*^{KO} strain. (**A**) Schematic representation of the upstream and downstream boundaries of 137 identified heterochromatin regions (spread longer than 1 kb) deduced from RIP index (52), whose positions are in alignment with that of panel B–E. (**B**–**E**) Metagene analyses display the normalized signals flanking the upstream and downstream boundaries of heterochromatin regions obtained from the WT and *dmm-1*^{KO} strains by HP1 ChIP-seq (B), 5mC profiles with WGBS(C), H2A.Z ChIP-seq (D) and H3K56ac ChIP-seq (E). To allow each of the 137 RIP relics to have the same weight in the metagene analyses, the signal of a given region, including full heterochromatin and flanking 3kb regions, are normalized by the max value of that region. The mean value of each position from 137 regions was calculated and plotted.

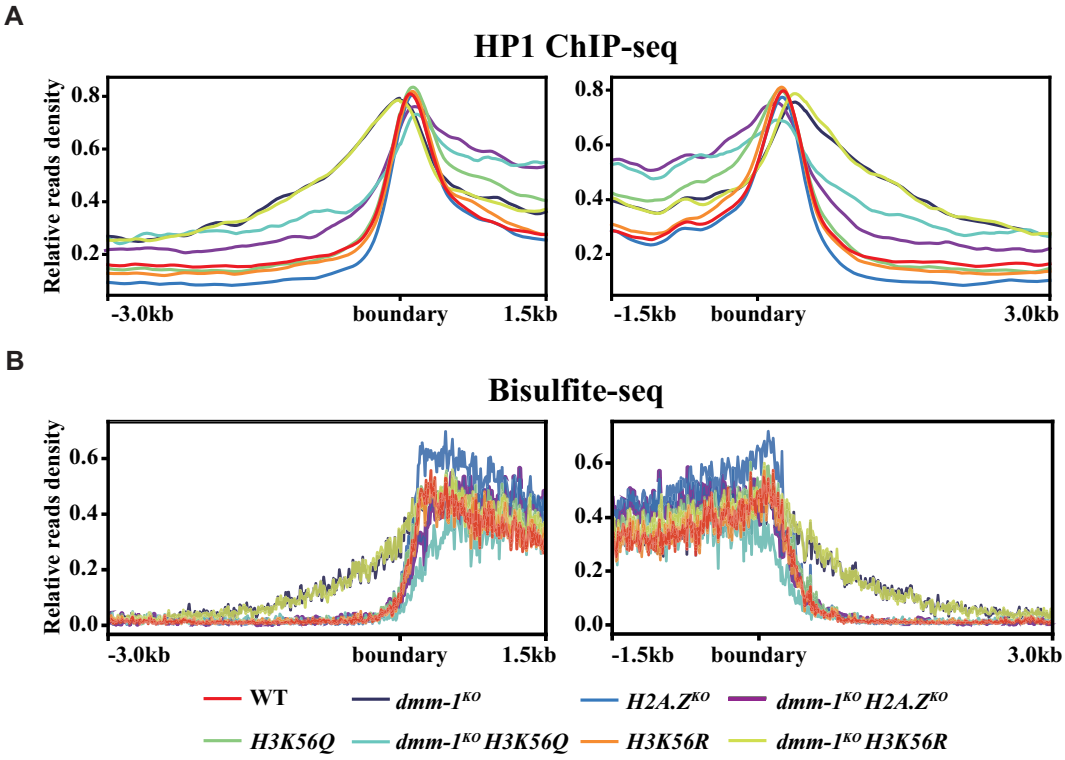

Figure 7. Loss of H2A.Z or mimicking H3K56 acetylation via an *H3K56Q* mutation effectively restricts aberrant heterochromatin spreading in the *N. crassa* genome. Metagene analyses display the distribution profiles of HP1 achieved by ChIP-seq (**A**) and DNA methylation (5mC) by WGBS (**B**) at the boundaries of 137 RIP relics in the WT, *dmm-1*^{KO}, *H2A.Z*^{KO}, *dmm-1*^{KO} *H2A.Z*^{KO}, *H3K56Q*, *dmm-1*^{KO} *H3K56Q*, *H3K56R* and *dmm-1*^{KO} *H3K56R* strains. For each region, all signals are normalized by the max value of the given region. The value of each position in the metaplot is the mean of those from the 137 regions.

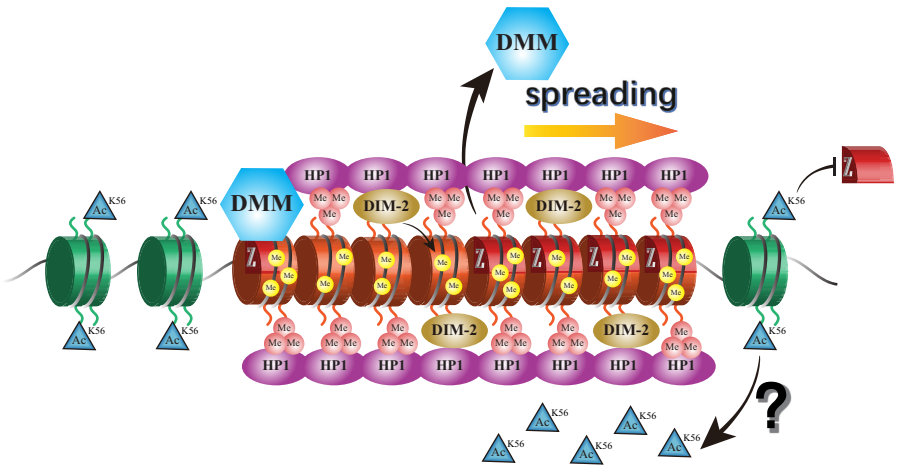

Figure 8. Model of aberrant heterochromatin spreading caused by DMM-1 deletion in *N. crassa*. When boundary protein DMM-1 is impaired, aberrant heterochromatin spreading can be initiated by removing H3K56 acetylation of adjacent euchromatic nucleosomes through an unknown mechanism, which facilitates H2A.Z incorporation. H2A.Z-containing nucleosomes may create a condensed chromatin environment and promote the spreading cycle of H3K9me3, HP1 and DNA methylation, eventually resulting in aberrant heterochromatin spreading and substantial euchromatic gene silencing.

The functions of H2A.Z in heterochromatin regulation

Unlike H3K56 acetylation, the diversified functions of H2A.Z in heterochromatin regulation have been extensively studied in different model organisms. In budding yeast, H2A.Z/Htz1 was shown to restrict Sir2-dependent heterochromatin spreading (21). However, investigation of HP1 and DNA methylation profiles in the *H2A.Z*^{KO} strain did not reveal any sign of heterochromatin spreading in this study. This result is not very surprising since *N. crassa* heterochromatin is very different than Sir2-dependent 'heterochromatin' and probably exploits different restriction mechanisms. In contrast, we found here that H2A.Z sharply

deposits at the expanded heterochromatin regions, and loss of H2A.Z blocks ectopic heterochromatin spreading, indicating that H2A.Z incorporation is a critical step for aberrant heterochromatin spreading caused by DMM-1 deletion in *N. crassa*. Similar functions were observed in other model organisms using H3K9me/HP1 systems to assemble heterochromatin, especially in mammals, where H2A.Z is enriched in heterochromatic foci with HP1α on the chromosomal arms and deletion of H2A.Z disrupts normal HP1α-chromatin interactions, notably at pericentric regions (61–63). In addition, co-localization of H2A.Z and DNA methylation on the spreading path in the *dmm-1*^{KO} strain indicated that they are not always mutually antagonistic chromatin marks as in the mammal or *A. thaliana* genome (64–66). Convincingly, genome-wide analysis in yeast demonstrated widespread decrease of H2A.Z levels in mutants with hyperacetylated H3K56 (49), consistent with the antagonism between H3K56 acetylation and H2A.Z deposition in our study.

Interestingly, H2A.Z participates in heterochromatin spreading outside of the boundaries in the *dmm-1*^{KO} mutant but is excluded from the interior of the heterochromatin in the WT strain. The peculiar AT-richness of *N. crassa* heterochromatin may also be the major reason for H2A.Z's lack of role in the middle of heterochromatin. Aberrant spreading of heterochromatin at adjacent euchromatin regions may require chromatin remodeling or histone variants incorporation owing to the low AT-richness, in which H2A.Z deposition has been shown to support a condensed chromatin environment (62). In addition, H2A.Z has been reported to be post-translationally modified by acetylation, methylation and monoubiquitination (67–69). Among these, acetylated H2A.Z is associated with transcriptional activation and heterochromatin boundaries, whereas methylated and monoubiquitinated H2A.Z are generally related to transcriptional silencing (67,69–72). Therefore, distinguishing the type of H2A.Z modifications in the WT and *dmm-1*^{KO} strains may explain this phenomenon in *N. crassa*.

To date, H3K56 acetylation and H2A.Z have been extensively reported in model organisms. Considering their conservative natures, further analyses will be necessary to determine whether similar regulatory mechanisms exist in other organisms.

DATA AVAILABILITY

Complete ChIP-seq and WGBS files have been deposited in NCBI's Gene Expression Omnibus (GEO; http://ncbi.nlm.nih.gov/geo) and are accessible through GEO Series accession number GSE193075.

SUPPLEMENTARY DATA

Supplementary Data are available at NAR Online.

ACKNOWLEDGEMENTS

We are very grateful to Prof. Yi Liu and Mr. Yubo He for the crucial revision of this manuscript.

FUNDING

National Key R&D Program of China [2018YFA0900500 to Q.H.]; National Natural Science Foundation of China [31771383 to Q.H.]; National Natural Science Foundation of China [31871254 to Y.K.D.]. Funding for open access charge: National Key R&D Program of China [2018YFA0900500 to Q.H.]; National Natural Science Foundation of China [31771383 to Q.H.]; National Natural Science Foundation of China [31871254 to Y.K.D.].
Conflict of interest statement. None declared.

REFERENCES

1. Beisel,C. and Paro,R. (2011) Silencing chromatin: comparing modes and mechanisms. *Nat. Rev. Genet.*, **12**, 123–135.
2. Grewal,S.I. and Jia,S. (2007) Heterochromatin revisited. *Nat. Rev. Genet.*, **8**, 35–46.
3. Hermann,J.M. (1930) Types of visible variations induced by X-rays in *Drosophila*. *J. Genet.*, **22**, 299–334.
4. Elgin,S.C. and Reuter,G. (2013) Position-effect variegation, heterochromatin formation, and gene silencing in *Drosophila*. *Cold Spring Harb. Perspect. Biol.*, **5**, a017780.
5. Geutjes,E.J., Bajpe,P.K. and Bernards,R. (2012) Targeting the epigenome for treatment of cancer. *Oncogene*, **31**, 3827–3844.
6. Sharma,S., Kelly,T.K. and Jones,P.A. (2010) Epigenetics in cancer. *Carcinogenesis*, **31**, 27–36.
7. Allshire,R.C. and Madhani,H.D. (2018) Ten principles of heterochromatin formation and function. *Nat. Rev. Mol. Cell Biol.*, **19**, 229–244.
8. Gaszner,M. and Felsenfeld,G. (2006) Insulators: exploiting transcriptional and epigenetic mechanisms. *Nat. Rev. Genet.*, **7**, 703–713.
9. Valenzuela,L. and Kamakaka,R.T. (2006) Chromatin insulators. *Annu. Rev. Genet.*, **40**, 107–138.
10. Rusche,L.N., Kirchmaier,A.L. and Rine,J. (2003) The establishment, inheritance, and function of silenced chromatin in *Saccharomyces cerevisiae*. *Annu. Rev. Biochem.*, **72**, 481–516.
11. Talbert,P.B. and Henikoff,S. (2006) Spreading of silent chromatin: inaction at a distance. *Nat. Rev. Genet.*, **7**, 793–803.
12. Kueng,S., Oppikofer,M. and Gasser,S.M. (2013) SIR proteins and the assembly of silent chromatin in budding yeast. *Annu. Rev. Genet.*, **47**, 275–306.
13. Wang,J., Lawry,S.T., Cohen,A.L. and Jia,S. (2014) Chromosome boundary elements and regulation of heterochromatin spreading. *Cell. Mol. Life Sci.*, **71**, 4841–4852.
14. Xu,F., Zhang,Q., Zhang,K., Xie,W. and Grunstein,M. (2007) Sir2 deacetylates histone H3 lysine 56 to regulate telomeric heterochromatin structure in yeast. *Mol. Cell*, **27**, 890–900.
15. Bi,X. and Broach,J.R. (1999) UASrpg can function as a heterochromatin boundary element in yeast. *Genes Dev.*, **13**, 1089–1101.
16. Donze,D., Adams,C.R., Rine,J. and Kamakaka,R.T. (1999) The boundaries of the silenced *HMR* domain in *Saccharomyces cerevisiae*. *Genes Dev.*, **13**, 698–708.
17. Fourel,G., Revardel,E., Koering,C.E. and Gilson,E. (1999) Cohabitation of insulators and silencing elements in yeast subtelomeric regions. *EMBO J.*, **18**, 2522–2537.
18. Bi,X. and Broach,J.R. (2001) Chromosomal boundaries in *S. cerevisiae*. *Curr. Opin. Genet. Dev.*, **11**, 199–204.
19. Kimura,A., Umehara,T. and Horikoshi,M. (2002) Chromosomal gradient of histone acetylation established by Sas2p and Sir2p functions as a shield against gene silencing. *Nat. Genet.*, **32**, 370–377.
20. Suka,N., Luo,K. and Grunstein,M. (2002) Sir2p and Sas2p opposingly regulate acetylation of yeast histone H4 lysine16 and spreading of heterochromatin. *Nat. Genet.*, **32**, 378–383.
21. Meneghini,M.D., Wu,M. and Madhani,H.D. (2003) Conserved histone variant H2A.Z protects euchromatin from the ectopic spread of silent heterochromatin. *Cell*, **112**, 725–736.
22. Rountree,M.R. and Selker,E.U. (2010) DNA methylation and the formation of heterochromatin in *Neurospora crassa*. *Heredity (Edinb)*, **105**, 38–44.

23. Lewis,Z.A., Honda,S., Khlafallah,T.K., Jeffress,J.K., Freitag,M., Mohn,F., Schubeler,D. and Selker,E.U. (2009) Relics of repeat-induced point mutation direct heterochromatin formation in *Neurospora crassa*. *Genome Res.*, **19**, 427–437.
24. Lewis,Z.A., Adhvaryu,K.K., Honda,S., Shiver,A.L., Knip,M., Sack,R. and Selker,E.U. (2010) DNA methylation and normal chromosome behavior in *Neurospora* depend on five components of a histone methyltransferase complex, DCDC. *PLoS Genet.*, **6**, e1001196.
25. Tamaru,H. and Selker,E.U. (2001) A histone H3 methyltransferase controls DNA methylation in *Neurospora crassa*. *Nature*, **414**, 277–283.
26. Zhao,Y., Shen,Y., Yang,S., Wang,J., Hu,Q., Wang,Y. and He,Q. (2010) Ubiquitin ligase components Cullin4 and DDB1 are essential for DNA methylation in *Neurospora crassa*. *J. Biol. Chem.*, **285**, 4355–4365.
27. Xu,H., Wang,J.Y., Hu,Q.W., Quan,Y., Chen,H.J., Cao,Y.Q., Li,C.B., Wang,Y. and He,Q. (2010) DCAF26, an adaptor protein of Cul4-based E3, is essential for DNA methylation in *Neurospora crassa*. *PLoS Genet.*, **6**, e1001132.
28. Kouzminova,E. and Selker,E.U. (2001) *dim-2* encodes a DNA methyltransferase responsible for all known cytosine methylation in *Neurospora*. *EMBO J.*, **20**, 4309–4323.
29. Freitag,M., Hickey,P.C., Khlafallah,T.K., Read,N.D. and Selker,E.U. (2004) HP1 is essential for DNA methylation in *Neurospora*. *Mol. Cell*, **13**, 427–434.
30. Honda,S. and Selker,E.U. (2008) Direct interaction between DNA methyltransferase DIM-2 and HP1 is required for DNA methylation in *Neurospora crassa*. *Mol. Cell. Biol.*, **28**, 6044–6055.
31. Storck,W.K., Bicocca,V.T., Rountree,M.R., Honda,S., Ormsby,T. and Selker,E.U. (2020) LSD1 prevents aberrant heterochromatin formation in *Neurospora crassa*. *Nucleic Acids Res.*, **48**, 10199–10210.
32. Honda,S., Lewis,Z.A., Huarte,M., Cho,L.Y., David,L.L., Shi,Y. and Selker,E.U. (2010) The DMM complex prevents spreading of DNA methylation from transposons to nearby genes in *Neurospora crassa*. *Genes Dev.*, **24**, 443–454.
33. Ayoub,N., Noma,K., Isaac,S., Kahan,T., Grewal,S.I. and Cohen,A. (2003) A novel jmjC domain protein modulates heterochromatization in fission yeast. *Mol. Cell. Biol.*, **23**, 4356–4370.
34. Zofall,M. and Grewal,S.I. (2006) Swi6/HP1 recruits a JmjC domain protein to facilitate transcription of heterochromatic repeats. *Mol. Cell*, **22**, 681–692.
35. Tsukada,Y., Fang,J., Erdjument-Bromage,H., Warren,M.E., Borchers,C.H., Tempst,P. and Zhang,Y. (2006) Histone demethylation by a family of JmjC domain-containing proteins. *Nature*, **439**, 811–816.
36. Wang,J., Tadeo,X., Hou,H., Tu,P.G., Thompson,J., Yates,J.R. and Jia,S. (2013) Epe1 recruits BET family bromodomain protein Bdf2 to establish heterochromatin boundaries. *Genes Dev.*, **27**, 1886–1902.
37. Wang,Y., Dong,Q., Ding,Z., Gai,K., Han,X., Kaleri,F.N., He,Q. and Wang,Y. (2016) Regulation of *Neurospora* Catalase-3 by global heterochromatin formation and its proximal heterochromatin region. *Free Radic. Biol. Med.*, **99**, 139–152.
38. Dong,Q., Wang,Y., Qi,S., Gai,K., He,Q. and Wang,Y. (2018) Histone variant H2A.Z antagonizes the positive effect of the transcriptional activator CPC1 to regulate *catalase-3* expression under normal and oxidative stress conditions. *Free Radic. Biol. Med.*, **121**, 136–148.
39. Belden,W.J., Larrondo,L.F., Froehlich,A.C., Shi,M., Chen,C.H., Loros,J.J. and Dunlap,J.C. (2007) The *band* mutation in *Neurospora crassa* is a dominant allele of *ras-1* implicating RAS signaling in circadian output. *Genes Dev.*, **21**, 1494–1505.
40. He,Q., Cha,J., He,Q., Lee,H.C., Yang,Y. and Liu,Y. (2006) CKI and CKII mediate the FREQUENCY-dependent phosphorylation of the WHITE COLLAR complex to close the *Neurospora* circadian negative feedback loop. *Genes Dev.*, **20**, 2552–2565.
41. Yang,S., Li,W., Qi,S., Gai,K., Chen,Y., Suo,J., Cao,Y., He,Y., Wang,Y. and He,Q. (2014) The highly expressed methionine synthase gene of *Neurospora crassa* is positively regulated by its proximal heterochromatic region. *Nucleic Acids Res.*, **42**, 6183–6195.
42. Livak,K.J. and Schmittgen,T.D. (2001) Analysis of relative gene expression data using real-time quantitative PCR and the $2^{-\Delta\Delta CT}$ method. *Methods*, **25**, 402–408.
43. Langmead,B. and Salzberg,S.L. (2012) Fast gapped-read alignment with Bowtie 2. *Nat. Methods*, **9**, 357–359.
44. Zhang,Y., Liu,T., Meyer,C.A., Eeckhoute,J., Johnson,D.S., Bernstein,B.E., Nusbaum,C., Myers,R.M., Brown,M., Li,W. *et al.* (2008) Model-based analysis of ChIP-Seq (MACS). *Genome Biol.*, **9**, R137.
45. Ramirez,F., Ryan,D.P., Gruning,B., Bhardwaj,V., Kilpert,F., Richter,A.S., Heyne,S., Dundar,F. and Manke,T. (2016) deepTools2: a next generation web server for deep-sequencing data analysis. *Nucleic Acids Res.*, **44**, W160–W165.
46. Thorvaldsdottir,H., Robinson,J.T. and Mesirov,J.P. (2013) Integrative Genomics Viewer (IGV): high-performance genomics data visualization and exploration. *Brief. Bioinform.*, **14**, 178–192.
47. Krueger,F. and Andrews,S.R. (2011) Bismark: a flexible aligner and methylation caller for bisulfite-seq applications. *Bioinformatics*, **27**, 1571–1572.
48. Courtney,A.J., Kamei,M., Ferraro,A.R., Gai,K., He,Q., Honda,S. and Lewis,Z.A. (2020) Normal patterns of histone H3K27 methylation require the histone variant H2A.Z in *Neurospora crassa*. *Genetics*, **216**, 51–66.
49. Watanabe,S., Radman-Livaja,M., Rando,O.J. and Peterson,C.L. (2013) A histone acetylation switch regulates H2A.Z deposition by the SWR-C remodeling enzyme. *Science*, **340**, 195–199.
50. Masumoto,H., Hawke,D., Kobayashi,R. and Verreault,A. (2005) A role for cell-cycle-regulated histone H3 lysine 56 acetylation in the DNA damage response. *Nature*, **436**, 294–298.
51. Xu,F., Zhang,K. and Grunstein,M. (2005) Acetylation in histone H3 globular domain regulates gene expression in yeast. *Cell*, **121**, 375–385.
52. Margolin,B.S., Garrett-Engele,P.W., Stevens,J.N., Fritz,D.Y., Garrett-Engele,C., Metzenberg,R.L. and Selker,E.U. (1998) A methylated *Neurospora* 5S rRNA pseudogene contains a transposable element inactivated by repeat-induced point mutation. *Genetics*, **149**, 1787–1797.
53. Trewick,S.C., Minc,E., Antonelli,R., Urano,T. and Allshire,R.C. (2007) The JmjC domain protein Epe1 prevents unregulated assembly and disassembly of heterochromatin. *EMBO J.*, **26**, 4670–4682.
54. Braunstein,M., Rose,A.B., Holmes,S.G., Allis,C.D. and Broach,J.R. (1993) Transcriptional silencing in yeast is associated with reduced nucleosome acetylation. *Genes Dev.*, **7**, 592–604.
55. Lieb,J.D., Liu,X., Botstein,D. and Brown,P.O. (2001) Promoter-specific binding of Rap1 revealed by genome-wide maps of protein-DNA association. *Nat. Genet.*, **28**, 327–334.
56. Bi,X. (2002) Domains of gene silencing near the left end of chromosome III in *Saccharomyces cerevisiae*. *Genetics*, **160**, 1401–1407.
57. Jack,A.P., Bussemer,S., Hahn,M., Punzeler,S., Snyder,M., Wells,M., Csankovszki,G., Solovei,I., Schotta,G. and Hake,S.B. (2013) H3K56me3 is a novel, conserved heterochromatic mark that largely but not completely overlaps with H3K9me3 in both regulation and localization. *PLoS One*, **8**, e51765.
58. Cambareri,E.B., Jensen,B.C., Schabtach,E. and Selker,E.U. (1989) Repeat-induced G-C to A-T mutations in *Neurospora*. *Science*, **244**, 1571–1575.
59. Singer,M.J., Marcotte,B.A. and Selker,E.U. (1995) DNA methylation associated with repeat-induced point mutation in *Neurospora crassa*. *Mol. Cell. Biol.*, **15**, 5586–5597.
60. Miao,V.P., Freitag,M. and Selker,E.U. (2000) Short TpA-rich segments of the zeta-eta region induce DNA methylation in *Neurospora crassa*. *J. Mol. Biol.*, **300**, 249–273.
61. Rangasamy,D., Berven,L., Ridgway,P. and Tremethick,D.J. (2003) Pericentric heterochromatin becomes enriched with H2A.Z during early mammalian development. *EMBO J.*, **22**, 1599–1607.
62. Fan,J.Y., Rangasamy,D., Luger,K. and Tremethick,D.J. (2004) H2A.Z alters the nucleosome surface to promote HP1α-mediated chromatin fiber folding. *Mol. Cell*, **16**, 655–661.
63. Rangasamy,D., Greaves,I. and Tremethick,D.J. (2004) RNA interference demonstrates a novel role for H2A.Z in chromosome segregation. *Nat. Struct. Mol. Biol.*, **11**, 650–655.
64. Conerly,M.L., Teves,S.S., Diolaiti,D., Ulrich,M., Eisenman,R.N. and Henikoff,S. (2010) Changes in H2A.Z occupancy and DNA methylation during B-cell lymphomagenesis. *Genome Res.*, **20**, 1383–1390.
65. Zilberman,D., Coleman-Derr,D., Ballinger,T. and Henikoff,S. (2008) Histone H2A.Z and DNA methylation are mutually antagonistic chromatin marks. *Nature*, **456**, 125–129.

66. Zemach,A., McDaniel,I.E., Silva,P. and Zilberman,D. (2010) Genome-wide evolutionary analysis of eukaryotic DNA methylation. *Science*, **328**, 916–919.
67. Binda,O., Sevilla,A., LeRoy,G., Lemischka,I.R., Garcia,B.A. and Richard,S. (2013) SETD6 monomethylates H2AZ on lysine 7 and is required for the maintenance of embryonic stem cell self-renewal. *Epigenetics*, **8**, 177–183.
68. Ishibashi,T., Dryhurst,D., Rose,K.L., Shabanowitz,J., Hunt,D.F. and Ausio,J. (2009) Acetylation of vertebrate H2A.Z and its effect on the structure of the nucleosome. *Biochemistry*, **48**, 5007–5017.
69. Sarcinella,E., Zuzarte,P.C., Lau,P.N., Draker,R. and Cheung,P. (2007) Monoubiquitylation of H2A.Z distinguishes its association with euchromatin or facultative heterochromatin. *Mol. Cell. Biol.*, **27**, 6457–6468.
70. Babiarz,J.E., Halley,J.E. and Rine,J. (2006) Telomeric heterochromatin boundaries require NuA4-dependent acetylation of histone variant H2A.Z in *Saccharomyces cerevisiae*. *Genes Dev.*, **20**, 700–710.
71. Draker,R., Sarcinella,E. and Cheung,P. (2011) USP10 deubiquitylates the histone variant H2A.Z and both are required for androgen receptor-mediated gene activation. *Nucleic Acids Res.*, **39**, 3529–3542.
72. Millar,C.B., Xu,F., Zhang,K. and Grunstein,M. (2006) Acetylation of H2AZ Lys 14 is associated with genome-wide gene activity in yeast. *Genes Dev.*, **20**, 711–722.